Journal of Materials Chemistry A

ROYAL SOCIETY OF CHEMISTRY

PAPER

View Article Online
View Journal | View Issue

Check for updates

Cite this: J. Mater. Chem. A, 2024, 12, 20307

Physically entangled multifunctional eutectogels for flexible sensors with mechanically robust†

Qianwen Lu,[a] Hengfeng Li *[a] and Zhijian Tan *[b]

Received 22nd April 2024
Accepted 28th June 2024

DOI: 10.1039/d4ta02751e

rsc.li/materials-a

Ionically conducting eutectogels have gained popularity as temperature-tolerant and cost-effective substitutes for hydrogels and ionogels in flexible electronic devices. In this study, mechanically robust eutectogels with antibacterial properties were fabricated using a facile one-step process that relied solely on the physical entanglement of polymer chains. At low initiator concentrations, the vinyl monomers underwent radical polymerization in deep eutectic solvents (DESs), forming physically entangled and transparent eutectogels. The eutectogels exhibited excellent mechanical properties (tensile strength, elongation at break, and fracture energy of 8.04 MPa, 620.5%, and 28.69 ± 2.23 MJ m^{-3}, respectively), a strong adhesion force, excellent ionic conductivity (0.43 ± 0.07 S m^{-1}), and remarkable resistance to freezing and drying (−20 to 80 °C). Moreover, the eutectogels possessed superior self-healing abilities at room temperature without the need for external stimuli. As sensors, the fabricated eutectogels exhibited high sensitivity, thereby enabling the precise, real-time, and stable monitoring of human activities. The eutectogels have promising applications in wearable technology, healthcare devices, and human–computer interfaces.

1. Introduction

The growing demand for innovative electronic devices in certain fields, such as artificial intelligence, implantable technology, soft robotics, and wearable electronics, has prompted the development of robust and stretchable gels.[1,2] Such gels are designed to possess versatile integrated features, including transparency, self-healing, self-adhesion, high conductivity, and temperature tolerance.[3–5] Conventional gels that utilize water,[6–8] organic solvents, or ionic liquids as continuous phases encounter certain challenges, such as limited temperature resistance, low conductivity, lack of biocompatibility, and high production costs, which significantly hinder their practical applications.[9–11] As a rising class of soft materials, eutectogels have recently attracted the attention of the public and have joined the gel family. They are typically formed using polymer networks,[12–14] nanoparticles,[15,16] low-molecular-weight gelators,[17–20] and deep eutectic solvents (DESs).[21] Owing to the inherently high electrical conductivity, low volatility, thermal stability, and affordability of DESs,[22,23] eutectogels are excellent candidates as flexible ionic conductors, thus replacing conventional temperature-intolerant hydrogels and costly ionogels. Moreover, they hold great promise in various fields such as energy, electronics, and environmental science, offering limitless potential for future advances.[11,24–26]

Polymer gels possess unique three-dimensional (3D) network structures that expand when exposed to solvents. Their exceptional solvent absorption capability has resulted in their widespread application in diverse fields, including biomedical engineering and electronics.[3,27–30] Under mechanical loading, the existence of immobilized uneven cross-linking points resulted in stress concentration, rendering brittleness and inadequate mechanical strength, the limitations of most traditional polymer gels.[31] Thus, significant efforts have been made to incorporate reversible bonds, such as non-covalent and dynamic covalent bonds, into the polymer gel network. These reversible bonds can improve the mechanical performance of polymer gels through the energy dissipation function related to breaking cross-linking points, and the self-healing function allowed reconstruction of the reversible cross-linking points.[32–34] Polymer eutectogels exhibit 3D network architecture that swells upon the absorption of DESs. They possess desirable characteristics for technological applications, including exceptional ionic conductivity, excellent thermal and electrochemical stability, non-volatility, and cost-effectiveness.[35] They are widely recognized for their exceptional mechanical properties, ease of processing, and malleability.[36] Fan *et al.* developed a poly(1-vinylimidazole)-based eutectogel in a choline chloride (ChCl)–glycerol system.[14] Their eutectogels exhibited excellent stretchability (approximately 2300%) and self-healing, self-adhesive, and temperature-tolerant performances. Wang *et al.* prepared a poly(vinyl alcohol)-based

[a]School of Materials Science and Engineering, Central South University, Changsha 410083, Hunan, P. R. China. E-mail: lihf@csu.edu.cn

[b]Institute of Bast Fiber Crops, Chinese Academy of Agricultural Sciences, Changsha 410205, Hunan, P. R. China. E-mail: tanzhijian@caas.cn

† Electronic supplementary information (ESI) available. See DOI: https://doi.org/10.1039/d4ta02751e

eutectogel that exhibited excellent freeze resistance, conductivity, and toughness.[37] Chen *et al.* demonstrated recyclable and multi-environmentally suitable eutectogels comprising gelatin-strengthened poly(vinyl alcohol) and DESs.[38] Although numerous studies have promoted the use of eutectogels in sensing applications,[35,39–41] research on eutectogels with antibacterial properties and strain sensor functionality is limited, as indicated by the data in Table S1.†

In this study, a series of robust and antibacterial polymer eutectogels were formed solely by the physical entanglement of polymer chains. All the reagents were placed in one pot under ultraviolet (UV) irradiation for a short time; thus, the preparation process was convenient and rapid. The radical polymerization of acrylic acid (AA) monomers using a choline chloride catechol (CC) DES occurred in the presence of a low initiator concentration. Owing to the entanglement of polymer chains and the existence of aromatic benzene rings, the eutectogels exhibited superior mechanical properties, such as high tensile strength (8.04 MPa), high fracture energy (28.69 ± 2.23 MJ m^{-3}), and high elongation at break (620.5%). They also exhibited excellent self-healing abilities at ambient temperatures without the need for external stimuli because of the reformation of polymer entanglements across the impaired interfaces. Computational simulations revealed the significant impact of the polymer–solvent interactions on the self-healing capacity of the eutectogels. Moreover, the prepared eutectogel exhibited a strong adhesive force on different surfaces, including skin, and excellent temperature tolerance, indicating that they can be used in harsh environments (cold and dry). The exceptional performance of the eutectogels rendered it highly suitable for human sensing applications, such as in flexible and wearable devices. Moreover, the simple one-step preparation process was affordable and did not require specially synthesized functional groups.

2. Experimental section

2.1 Materials

Acrylic acid (AA), choline chloride (ChCl), catechol (Ca), resorcinol (Re), hydroquinone (Hy), ethyl acetate (EA), poly(ethylene glycol) diacrylate (crosslinker, PEGDA, average M_n of approximately 400), and 2-hydroxy-2-methylpropiophenone (photoinitiator, Irgacure 1173) were purchased from Aladdin Biochemical Technology Co., Ltd (Shanghai, China). ChCl was added after vacuum drying overnight. Ca, Re, and Hy were decolorized and recrystallized with activated carbon and EA before use to obtain white products (Fig. S1†). Cefotaxime sodium (CS) was purchased from Beijing Dingguo Biotechnology Co., Ltd (China). Medical polyurethane (PU) films were obtained online.

2.2 Preparation of DESs

ChCl–Ca (CC) DES was prepared by mixing ChCl and Ca at a molar ratio of 1 : 2, followed by stirring at 80 °C for 2 h to form a homogeneous and colorless liquid. Five other DESs were prepared using a similar procedure and are listed in Table S2.†

2.3 Fabrication of the PAA/CC eutectogels

The PAA/CC eutectogels were prepared as follows. Briefly, AA (4.0 g), CC (6.0 g), PEGDA (0 g), and Irgacure 1173 (40 mg) were added to a centrifuge tube. The tube was then placed on a high-speed vortex oscillator to evenly stir the liquid. Subsequently, the mixed solution was ultrasonicated for 10 min to remove bubbles. Finally, the mixture was poured into a Teflon mold and irradiated with UV light for 10 min. This process was conducted at room temperature under atmospheric conditions. Other eutectogels were prepared using similar methods, as listed in Tables S3 and S4.† Based on the DES composition, the eutectogels were named PAA/CC-1, PAA/CC, PAA/CR-1, PAA/CR, PAA/CH-1, and PAA/CH, respectively. For different contents of CC and PEGDA contents, the eutectogels were labeled PAA/CC$_x$P$_y$ (x = 50, 60, and 70, denoting CC contents of 50%, 60%, and 70%, respectively (w/w); y = 0.1, 0.25, 0.5, 0.75, and 1.0, denoting that the added amounts of PEGDA were 0.1%, 0.25%, 0.5%, 0.75%, and 1.0% of AA (mol/mol), respectively). When PEGDA was not added, there was no P in the name. Notably, PAA/CC represented a CC content of 60 wt% with no PEGDA addition. The PAA hydrogel was prepared by replacing the CC DES with deionized water, without the addition of PEGDA.

Additional information regarding the experiment is provided in the ESI.†

3. Results and discussion

3.1 Fabrication and characterization of the PAA/CC eutectogels

A series of eutectogels were fabricated *via* one-step polymerization. Briefly, a 1 : 2 (mol/mol) CC DES was evenly mixed with AA and Irgacure 1173, promoting electrostatic interactions, van der Waals forces, and hydrogen bonding, and then used for copolymerization *via* UV radiation (Fig. 1a). The obtained eutectogels were named PAA/CC$_x$P$_y$ (where x denotes the CC content and y denotes the amount of the crosslinking agent, PEGDA). Polymerization with the addition of the PEGDA crosslinker resulted in irreversible chemical crosslinking networks in the PAA, as shown in Fig. S2,† which did not obstruct the reversible non-covalent linking between PAA and CC. Theoretical simulation calculations were performed to analyze the interactive mode of PAA/CC. The independent gradient model (IGM) was used to show the size of the interaction, and the cohesive energy density (CED) was applied to demonstrate the energy density per unit volume in PAA/CC (more detailed modeling information is presented in the ESI†).[42,43] As depicted in Fig. 1b, S3, S4 and Table S5,† the IGM analysis indicated that the PAA/CC polymer network exhibited low interaction energy (-29.01 kcal mol^{-1}) that was primarily due to strong attractive interactions, such as hydrogen bonding and electrostatic interactions. Additionally, PAA/CC exhibited a high CED of 1.718×10^9 J m^{-3}. Five types of eutectogels, PAA/CC$_{60}$-1, PAA/CR$_{60}$-1, PAA/CR$_{60}$, PAA/CH$_{60}$-1, and PAA/CH$_{60}$, were prepared using a similar procedure, as indicated in Tables S3 and S4.† The PAA/CC eutectogel exhibited excellent transparency >80% at 400–800 nm (Fig. S7†).

The FTIR and ^{1}H NMR spectra clearly indicated the successful preparation of the CC DES and PAA/CC eutectogel,

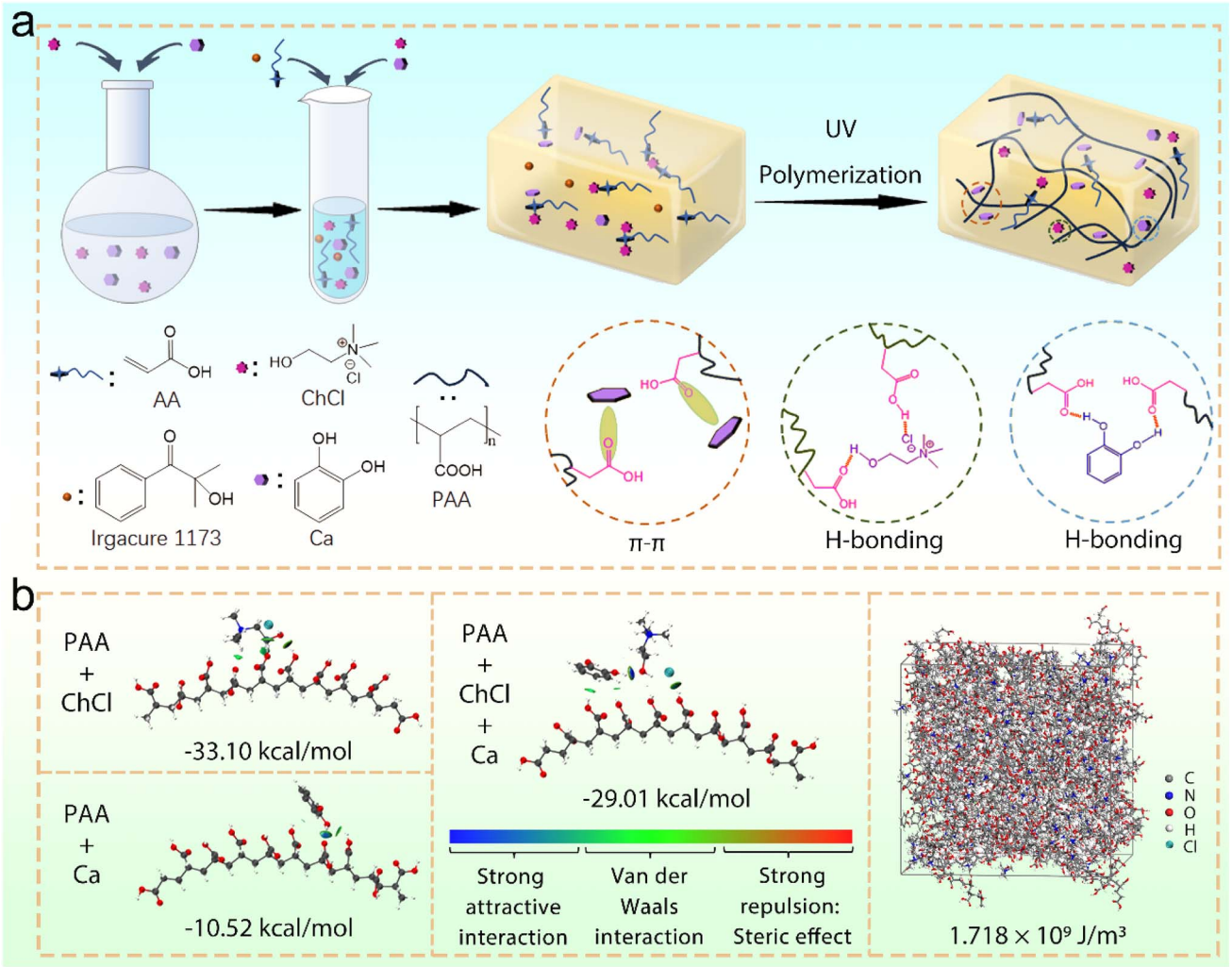

Fig. 1 (a) Schematic diagram of the PAA/CC eutectogel fabrication process. (b) Independent gradient model (IGM) isosurfaces between PAA, ChCl, and Ca, and the cohesive energy density (CED) of PAA/CC (CC content of 60 wt%; 50 PAA molecules, 150 ChCl molecules, and 300 Ca molecules).

and no covalent interactions were observed between AA and CC (Fig. S5 and S6†). Thus, the linear PAA and CC DES agent were probably two independent but interconnected structures in the PAA/CC system, connected by non-covalent interactions, such as hydrogen bonding, π–π, cation–π, and electrostatic interactions.[44] As shown in Fig. S5,† compared with PAA/CC, the $\nu_{C=O}$ of the carboxyl group in PAA (1700 cm^{-1}) shifted to 1713 cm^{-1}, and the γ_{C-H} of the C–H out of plane bending vibration in the benzene ring ortho disubstituted system in CC (744 cm^{-1}) shifted to 750 cm^{-1}, indicating the hydrogen bonding interactions between PAA and CC. As demonstrated in Fig. S6,† signals corresponding to the protons in the phenyl group were observed, indicating that both the CC DES and PAA/CC eutectogels were successfully prepared. These results were consistent with the simulation results.

3.2 Mechanical properties of the PAA/CC eutectogels

The mechanical properties of the PAA/CC eutectogels were evaluated using tensile tests. The tensile strength, elongation at break, and fracture energy of PAA/CC were 8.04 MPa, 620.5%, and 28.69 ± 2.23 MJ m^{-3}, respectively. Additionally, PAA/CC reached a compressive stress (16.27 MPa) at 82.2% strain (Fig. S8†). The presence of benzene rings in Ca probably contributed to the mechanical properties of PAA/CC, because benzene rings typically enhance the strength and toughness of materials while often reducing their elongation. These values were the highest among those of the six eutectogels and surpassed those of most reported stretchable ionic conductors, as shown in Fig. 2a, S10a and Table S3.† These properties can prevent the piercing of blunt weapons (Fig. S9†). Notably, Ca exhibited the lowest toxicity among the three dihydroxybenzene compounds and showed inhibitory activity against bacteria and dermatophytes, rendering it a viable candidate for use in wearable devices. When the PEGDA crosslinker was added to the copolymerization system, the tensile strength and elongation at break decreased (Fig. 2b, S10b and Table S4†). This was primarily attributed to the addition of PEGDA, which introduced an irreversible crosslinking network of PAA, thereby

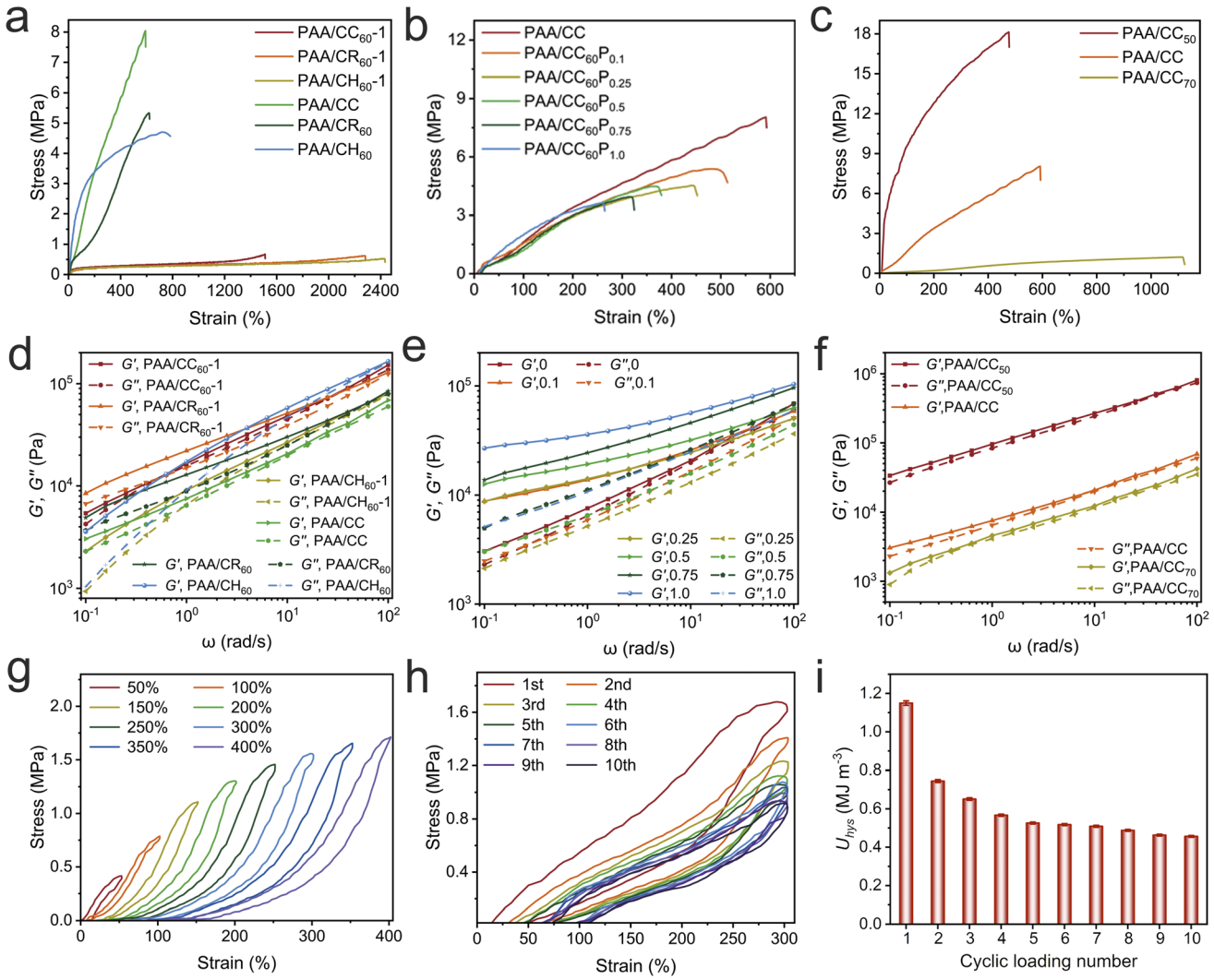

Fig. 2 Mechanical properties of the eutectogels. (a, and d) Tensile strain–stress curves and rheological tests of the six eutectogels. (b, and e) Tensile strain–stress curves and rheological tests of PAA/$CC_{60}P_y$ (y = 0, 0.1, 0.25, 0.5, 0.75 and 1.0 represent the additional crosslinking agent amounts of 0%, 0.1%, 0.25%, 0.5%, 0.75% and 1.0% (mol/mol) of AA, respectively). (c, and f) Tensile strain–stress curves and rheological tests of PAA/CC_x (x = 50, 60, and 70 denote the CC content as 50%, 60%, and 70% (w/w), respectively). (g) Tensile strain–stress diagrams of PAA/CC at various levels of strain. (h) Consecutive cyclic loading plots of PAA/CC subjected to a strain of 300%. (i) Dissipated energy (U_{hys}) of PAA/CC throughout successive loading cycles under a tensile strain of 300%.

limiting the π–π interaction between Ca and PAA and hindering the movement of the polymer chains.[45] By adjusting the CC content, the mechanical properties of PAA/CC could be changed (Fig. 2c, S10c and Table S4†). For example, with increasing CC content, the tensile strength of PAA/CC decreased from 18.14 to 1.22 MPa, and the elongation at break increased from 525.5% to 1149%. These prominent changes were primarily caused by increased hydrogen bonding and π–π interactions within the eutectogels with increasing CC content. Thus, the synergistic effect of these two non-covalent physical interactions resulted in an increase in the tensile strength of the PAA/CC eutectogels. Moreover, the toughness of PAA/CC decreased from 60.96 ± 1.33 MJ to 6.36 ± 1.32 MJ m^{-3}. This decrease was attributed to the increasing CC content improving energy dissipation through additional hydrogen bond breakage during the tensile process.[46] This ability to enhance the strength and toughness of gels while increasing the CC content is an ideal feature for designing advanced materials.

Rheological tests confirmed that all the fabricated eutectogels exhibited typical elastic behavior, with a storage modulus (G') > the loss modulus (G''), as illustrated in Fig. 1d–f.[19] Furthermore, the six eutectogels possessed excellent ionic conductivity (Fig. S11 and Table S3†). PAA/CC_{60}-1 exhibited the highest ionic conductivity (1.42 ± 0.06 S m^{-1}), whereas PAA/CC exhibits the lowest (0.43 ± 0.07 S m^{-1}). As depicted in Fig. S11 and Table S4,† the eutectogels with different CC contents and various amounts of PEGDA also demonstrated good ionic conductivity. Thus, the higher the toughness of the eutectogel, the lower the ionic conductivity. Eutectic ionic conductive gels, which are known for their excellent mechanical properties, are highly promising options for use in flexible electronic devices.[47] Based on the results of this study, PAA/CC with no added

PEGDA and a CC content of 60 wt% was selected for follow-up investigations. The eutectogel was physically entangled.

Cyclic stretch–release tests were performed to further confirm the excellent elasticity and capacity for self-recovery of PAM/CC. As depicted in Fig. 2g, during each loading–unloading cycle of incremental strain, PAA/CC exhibited recovery, underscoring its self-restoration capability attributed to the dynamic attributes of non-covalent bonding interactions.[19] The effective energy dissipation of PAA/CC was evaluated using ten consecutive loading–unloading tests at a strain of 300%, as depicted in Fig. 2h and i. As shown in Fig. 2i, a steep decline occurred in the dissipation energy after the initial cycle, followed by gradual stabilization within the second to tenth cycle. This trend highlighted enhanced elastic recovery, which could be attributed to the presence of reversible hydrogen bonds formed within PAA/CC,[46] which exhibited susceptibility to disruption under stress yet swiftly reformed upon stress release. This phenomenon enabled the elongated polymer chains to revert to their initial state, effectively protecting the integrity of the gel network from potential damage and indicating extraordinary elasticity and endurance.[21]

3.3 Adhesion and self-healing properties of the PAA/CC eutectogels

The excellent adhesive property of the eutectogels endowed the sensor with a solid and steady attachment to the electrode and underlying substrate. Moreover, it prevented the application of external auxiliary media with high interface resistance, thereby ensuring the stable and reliable function of eutectogels in flexible wearable electronic devices. As shown in Fig. 3a, b, S12 and Video S1,† PAA/CC displayed superior adhesion to different substrates, including glass, iron, copper, poly(methyl methacrylate) [PMMA], polytetrafluoroethylene [PTFE], and human skin. The PMMA plates adhered to PAA/CC and could withstand a weight of 10 kg without slippage (Fig. 3b). The PAA/CC that adhered to the human skin also exhibited excellent adhesive properties and could bear a large tensile deformation. The adhesion strengths were measured using a lap shear test.[21] Its adhesion strengths to iron, copper, glass, PMMA, and PTFE were 530.19 ± 84.69, 380.88 ± 18.80, 451.62 ± 95.81, 468.35 ± 73.34, and 80.88 ± 18.22 kPa, respectively (Fig. 3c). Moreover, the adhesive effects were well maintained under low-temperature (−20 °C) and high-temperature (80 °C) conditions. This was because PAA/CC possessed abundant carboxyl and hydroxyl groups and benzene rings, which enabled it to adhere to various substrates *via* multiple non-covalent bonding interactions, such as electrostatic attraction, ion–dipole interactions, hydrogen bonding, and metal coordination complexation.[46]

PAA/CC demonstrated a remarkable self-healing ability, which was confirmed through visual testing (Fig. 3d and Video S2†). The two gel segments were placed in contact at room temperature within a desiccator for 12 h without applying any external force, resulting in a PAA/CC healing efficiency of 72.71%. The other gels also exhibited significant healing effects, as shown in Fig. 3f, g, S13 and Tables S3 and S4.† This was due to the physical cross-linking of the polymer network. Furthermore, the step–strain sweep test provided additional evidence for the rapid and reversible gel–sol–gel transition observed in PAA/CC under alternating high-strain (100%) and low-strain (0.1%) conditions, thus highlighting its impressive thixotropic properties and self-healing ability (Fig. 3e). The other eutectogels also exhibited good self-recovery properties (Fig. S14–S16†).

The carboxyl groups of AA could function as both hydrogen bond acceptors and donors. The self-healing behavior observed in this system could be attributed to the hydrogen bonds formed between the carboxyl groups of the polymer chain, hydroxyl groups of Ca and ChCl, and quaternary ammonium salt group of ChCl (Fig. 1a). Additionally, the π–π interactions between the carbonyl groups of the polymer chain and the benzene rings of Ca might also significantly contribute to the self-healing mechanism, as depicted in Fig. 1a. This hypothesis was supported by the FTIR analysis (Fig. S5†) and simulation results shown in Fig. 1b. The eutectogel system provided reversible hydrogen bond structures and π–π interactions between the carboxyl groups and DES solvent. During the healing process, the DES solvent molecules transiently spread and interacted with the polymer chains, reestablishing hydrogen bonds and π–π interactions, thereby facilitating the repair of the eutectogels. Based on this analysis, a plausible self-healing mechanism for PAA/CC was proposed, as depicted in Fig. 3h.

3.4 Temperature-tolerance and antibacterial properties of the PAA/CC eutectogels

Benefiting from the low freezing point and non-volatile nature of DESs, the PAA/CC eutectogels exhibited impressive anti-freezing and anti-drying properties. They also exhibited excellent stretchability from −20 to 80 °C (Fig. 4a) after storage at different temperatures for 24 h. The rheological evaluation revealed the elasticity of PAA/CC across a wider temperature range of 25 to 110 °C (Fig. 4b). The other eutectogels exhibited similar rheological behaviors (Fig. S17–S19†). Thermogravimetric analysis of the PAA/CC_xP_y eutectogels, including PAA/CC, revealed a minimal weight loss below 200 °C (Fig. S20†). These findings demonstrated the remarkable high-temperature resistance of PAA/CC. Differential scanning calorimetry (DSC) tests spanning from −100 to 100 °C revealed that incorporating CC into the PAA/CC eutectogels significantly decreased the glass transition temperature (T_g) from 48.59 °C (PAA) to −35.69 °C (Fig. 4c and Table S6†). This enhancement enabled improved processability at lower temperatures. Additionally, the T_g of PAA/CC measured using dynamic thermomechanical analysis was almost consistent with the DSC test results (Fig. S21†). These results demonstrated the outstanding ability of PAA/CC to resist freezing. Following storage at −20 and 80 °C for 24 h (Fig. S22† and Videos S3 and S4), PAA/CC could still bear a weight of 500 g, indicating good temperature tolerance. The excellent anti-freezing and anti-drying capabilities of PAA/CC render it desirable for the formulation of advanced materials.

Antibacterial properties are crucial for skin-attachable wearable electronics to ensure the well-being of individuals

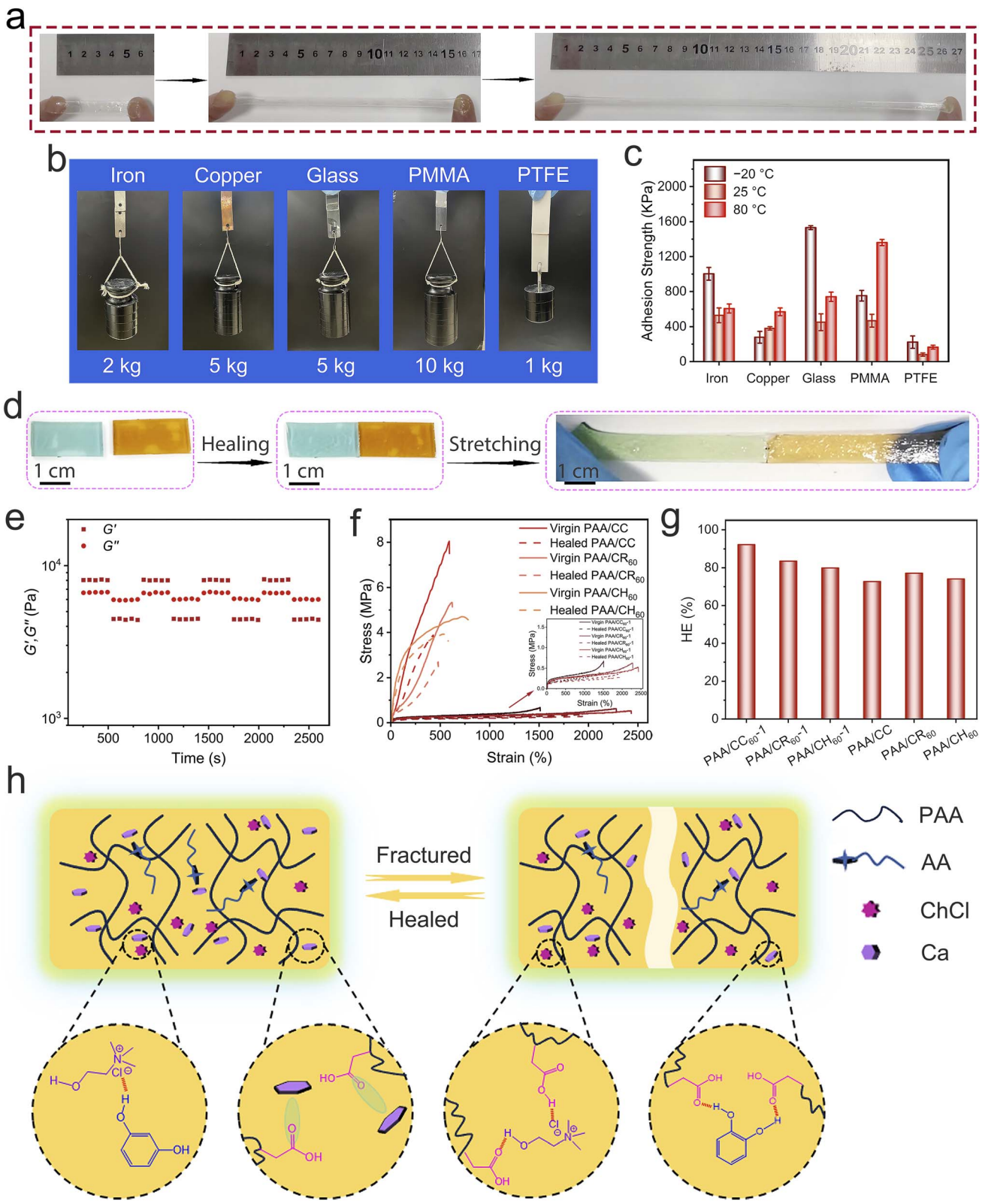

Fig. 3 Adhesive and self-healing properties of the PAA/CC eutectogel. (a) Photographs of PAA/CC adhered to the skin and stretched to deformation. (b) Photos of PAA/CC adhered to diverse substrates. (c) Adhesion strength of PAA/CC adhering to various substrates adhered at different temperatures. (d) Photograph of the self-healing ability of PAA/CC. (e) Rheological stepwise strain test of PAA/CC. (f) Tensile strain–stress curves of the six virgin and healed eutectogels. (g) Healing effectiveness (HE) of the six eutectogels. (h) Viable self-healing mechanism of PAA/CC in response to damage.

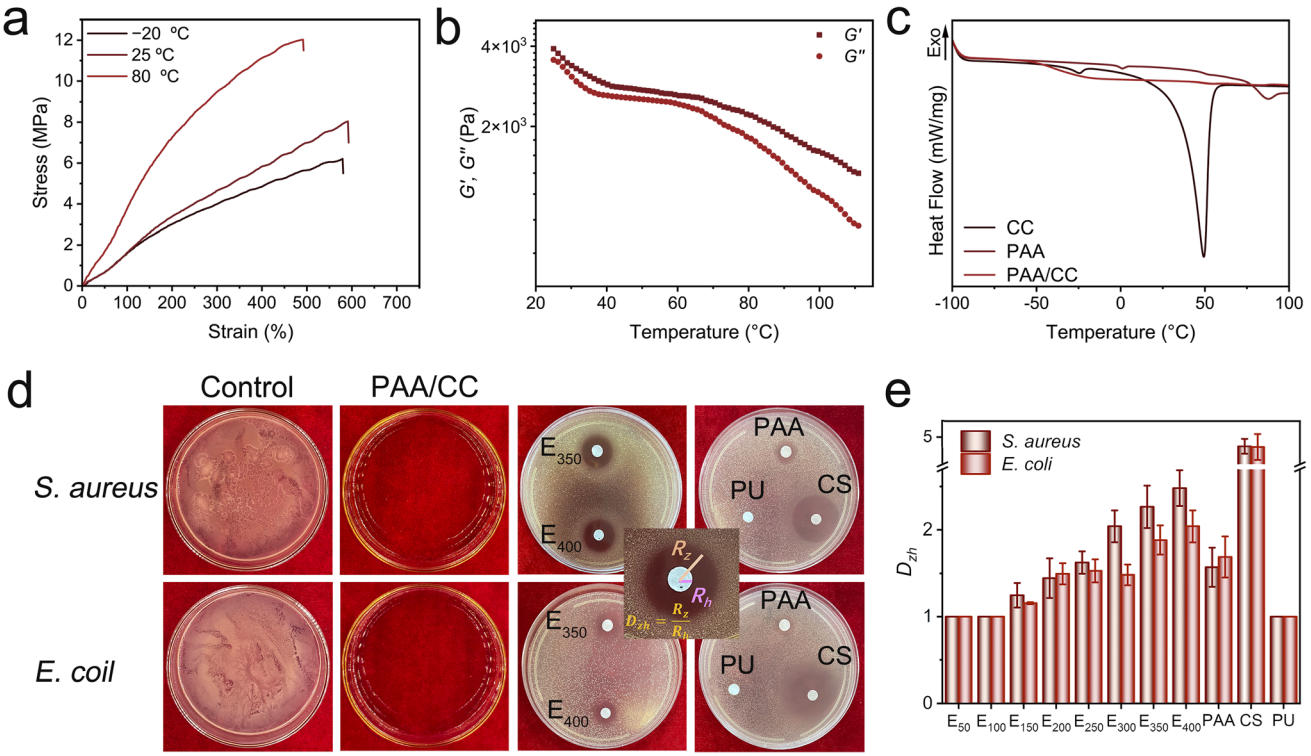

Fig. 4 Temperature-tolerance and antibacterial performance of PAA/CC. (a) Tensile strain–stress curves of PAA/CC following storage at different temperatures (−20, 25, and 80 °C) for 24 h. (b) Temperature ramp rheological test of PAA/CC with the temperature ranging from 25 to 110 °C. (c) DSC thermograms of the PAA hydrogel, PAA/CC eutectogel, and CC DES. (d) Antibacterial efficiencies of the PAA/CC, PAA/CC aqueous solutions (denoted as E_x, with concentrations of 350 and 400 mg mL^{-1}) filter papers, PAA hydrogel aqueous solution (400 mg mL^{-1}) filter papers, CS aqueous solution (500 ppm) filter papers, and medical polyurethane (PU) films against *S. aureus* and *E. coli*. (e) D_{zh} values of the PAA/CC eutectogel, PAA hydrogel, CS, and PU towards two types of bacteria.

because they protect the skin from potential external infections. The antibacterial properties of the PAA/CC eutectogel aqueous solution (E_x, x = 350 and 400 mg mL^{-1}), PAA hydrogel aqueous solution (400 mg mL^{-1}), cefotaxime sodium aqueous solution (CS, 500 ppm), and medical polyurethane (PU) film were evaluated against two common bacterial strains, *Staphylococcus aureus* (*S. aureus*) and *Escherichia coli* (*E. coli*), using the inhibition zone test (Fig. 4d and e). CS filter papers were used as positive controls and PU films were used as negative controls. D_{zh}, which is defined as R_z/R_h (the ratio of the radius of the bacteriostatic zone to the radius of the material), served as a quantitative measure of antibacterial efficacy. As shown in Fig. 4e, after 24 h of cultivation, the D_{zh} of PAA/CC (400 mg mL^{-1}) against *S. aureus* and *E. coli* were 2.48 ± 0.21 and 2.04 ± 0.18, respectively, whereas the negative control group exhibited a D_{zh} of 1, showing no antibacterial ability against the two bacteria. The D_{zh} values of PAA/CC (400 mg mL^{-1}) against *S. aureus* and *E. coli* were higher than those of PAA (400 mg mL^{-1}), which may be due to the synergy between PAA and Ca. Furthermore, the spread plate method was used to evaluate the antibacterial activity of PAA/CC. The results revealed that no bacteria grew on the PAA/CC plates; thus, PAA/CC effectively inhibited the growth of these two bacteria (Fig. 4d). Fungal inhibition tests were performed using PAA/CC (400 mg mL^{-1}) and PU (Fig. S23†). The inhibition (denoted as the ratio of the radius of the fungal reproduction zone to the radius of the media) of *Rhizoctonia solani Kuhn* (*R. solani*) and *Fusarium oxysporum* f. sp. *nelumbicola* (*F. oxysporum*) by PAA/CC (400 mg mL^{-1}) was 100% and 38.71% ± 2.39%, respectively. These results confirmed the remarkable ability of PAA/CC to inhibit various disease-causing bacteria and fungi.

3.5 Sensing performance of the PAA/CC eutectogels

A self-adhesive strain sensor was developed as a resistivity-type sensor to demonstrate the potential applications of the conductive PAA/CC eutectogel, which exhibited excellent adhesion and strain-induced resistance changes. In Fig. 5a, the resistance changes of the strain sensor based on PAA/CC are plotted against the applied strain, which increased up to 400%. The gauge factor (GF) quantified the strain sensitivity of the sensors, representing the relative resistance change concerning the applied strain ($(\Delta R/R_0)/\varepsilon$).[48,49] Fig. 5a illustrates the four distinct stages of the strain sensor response to increasing strain. Initially, the strain sensor exhibited a GF of 2.90 within the strain range of 0–100%. As the strain increased to 100–200%, the GF slightly increased to 4.28. Notably, the strain sensor demonstrated good sensitivity, with GF values of 2.62 and 3.58 in the strain ranges of 200–300% and 300–400%, respectively. Furthermore, the eutectogel-based sensor exhibited the ability to detect electrical signals within both low-strain (10–70%) and high-strain (100–400%) ranges (Fig. 5b and c). The amplitude of

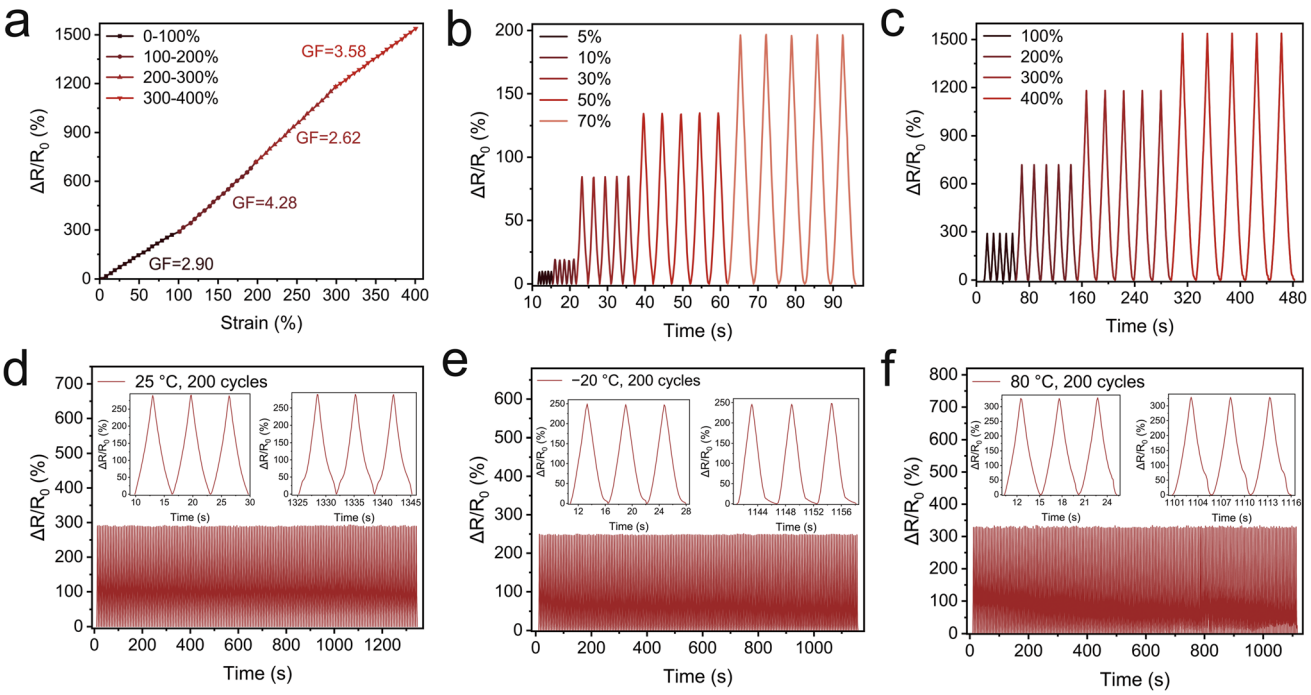

Fig. 5 Sensing performance of the PAA/CC eutectogel. (a) Variation in relative resistance with different levels of strain. (b, and c) Relationship between relative resistance and strain under various tensile cycles. (d–f) Changes in relative resistance at a 100% strain throughout 200 tensile cycles at temperatures of (d) 25, (e) −20, and (f) 80 °C.

the signal progressively increased with increasing strain levels. This demonstrated the excellent sensitivity, stability, and repeatability of the sensor for signal capture. Moreover, the strain sensor demonstrated remarkable stability and could endure up to 200 cycles under 100% strain (Fig. 5d). This was because of the superior anti-fatigue characteristics of PAA/CC. Even under extreme temperature conditions, such as sub-zero temperatures as low as −20 °C and high temperatures reaching up to 80 °C, the sensor maintained its stable performance (Fig. 5e and f). This ability was comparable to its performance at room temperature. As shown in Fig. 6a, the eutectogel sensor exhibited remarkable self-healing capabilities that could maintain comparable strain sensitivity even after healing. This unique characteristic rendered it an ideal choice for wearable sensors, thereby enabling the accurate and real-time detection of various human body movements. The strain sensor prepared in this study demonstrated remarkable stability and sensitivity to strain owing to its unique anti-freezing and solvent-retention properties. Its remarkable combination of high sensitivity, signal stability, self-healing capability, and resilience over a wide range of temperatures renders it an attractive choice for wearable sensor applications and holds great promise for this field.

The PAA/CC eutectogel was suitable for use as a wearable sensor because of its excellent sensitivity and stable signal output. It could accurately detect a wide range of body movements, both large-scale movements and subtle in real time. The PAA/CC eutectogel sensor effectively tracked the bending and stretching motions of the finger, wrist, knee, ankle, and elbow joints, showing steady signals (Fig. 6b–d, S24 and S25†). With the increase in finger bending angle (Fig. 6b), there was a stepwise rise in $\Delta R/R_0$ values. This could be attributed to the conformational stretching of the strain sensors. Notably, the $\Delta R/R_0$ response exhibited a positive correlation with the degree of bending. Thus, as the finger bent more, the change in resistance ($\Delta R/R_0$) recorded by the sensors increased accordingly. This was achieved by measuring the strength of ionic conductivity, which varied with the different bending angles. This simple yet effective mechanism enabled the sensor to provide reliable real-time monitoring of the finger movements. The PAA/CC eutectogel-based strain sensor offered intriguing bidirectional detection features that were not limited to convex surfaces. For example, the skin surface transitioned from convex to concave when moving in the opposite direction. Fig. 6c illustrates the strain sensor response when detecting continuous wrist bending in both the upward and downward directions. Consistently stable signals were obtained for both bending movements, and the $\Delta R/R_0$ variation accurately corresponded to the degree of bending. Similar results were observed when ankle movements, involving bending in two perpendicular directions, were detected (Fig. S22†). Moreover, the high sensitivity of the PAA/CC eutectogel sensor enabled it to be positioned on the forehead and pharynx of volunteers to detect subtle and intricate movements, including frowning and smiling (Fig. 6e and f). Morse code serves as a signaling system, which represents the 26 English letters using different combinations of dots and short dashes (Fig. 6g). Attaching a flexible sensor to the fingertip enabled the transmission of these dots and short dashes by quickly flexing the finger for dots and holding the finger for dashes. As a result, specific words such as

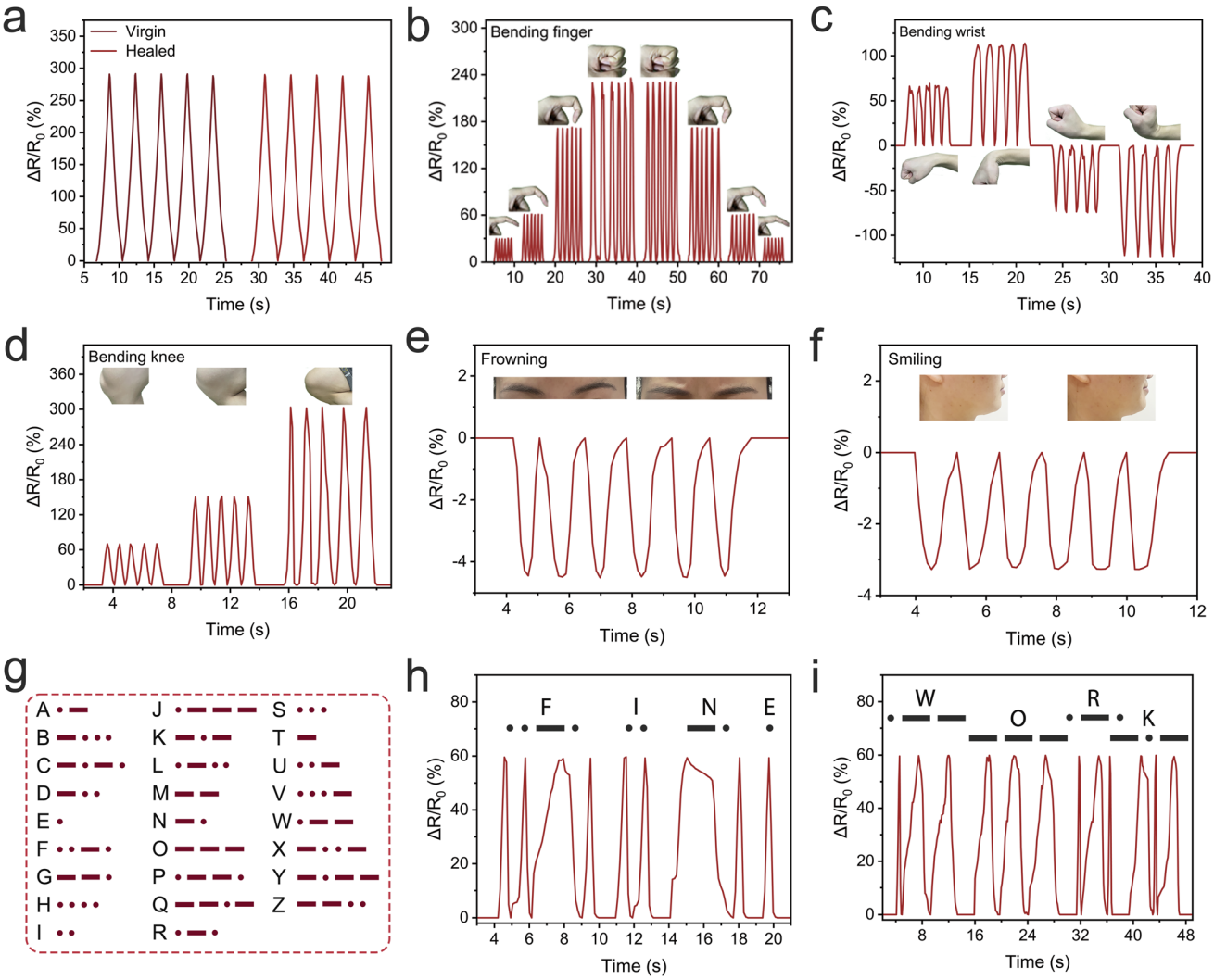

Fig. 6 Detection of motion by the PAA/CC sensors. (a) Relative resistance changes of both virgin and healed PAA/CC during the cyclic 100% strain process. (b–d) Monitoring large-scale movements: (b) bending finger, (c) wrist, and (d) knee. (e, and f) Monitoring subtle movements: (e) frowning and (f) smiling. (g) The Morse code signaling system corresponds to the 26 letters of the English alphabet. (h, and i) Output of Morse code words (h) "FINE" and (i) "WORK" by the strain sensor.

"FINE" and "WORK" could be formed and communicated (Fig. 6h and i). These findings confirmed the remarkable ability of the PAA/CC eutectogel sensor to effectively capture human movements and communicate information.

4. Conclusions

A physical approach for designing mechanically robust, self-healing, self-adhesive, antibacterial, and wide temperature-tolerant (−20 to 80 °C) eutectogels was proposed. The approach involved a simple one-step *in situ* polymerization of polymers in DESs. The eutectogel was constructed solely through the physical entanglement of the polymers in the DESs. Owing to their versatile design and superior performance, the polymer eutectogels have significant potential for use as wearable strain sensors. These sensors accurately detected diverse body movements (bidirectional monitoring) with high sensitivity and long-term stability. These eutectogels were distinct from previously reported polymeric eutectogel systems because they are formed purely through physical entanglement. This multifunctional material holds great promise for various applications in portable technologies and artificial electronic equipment.

Data availability

The data supporting this article have been included as part of the ESI.†

Conflicts of interest

The authors declare no competing financial interests.

Acknowledgements

This work was financially supported by the National Natural Science Foundation of China (no. 21878326), the Science and

Technology Innovation Program of Hunan Province-Huxiang Young Talent Program (no. 2021RC3116), the Training Program for Excellent Young Innovators of Changsha (no. kq2206073), the Agricultural Science and Technology Innovation Program (no. ASTIP-IBFC08), and the Earmarked Fund for the China Agriculture Research System (no. CARS-16-E24).

References

1 X. Zhang, W. Liu, J. Cai, J. Huang and X. Qiu, *J. Mater. Chem. A*, 2019, **7**, 26917–26926.
2 Q. Li, B. Tian, G. Tang, H. Zhan, J. Liang, P. Guo, Q. Liu and W. Wu, *J. Mater. Chem. A*, 2024, **12**, 3589–3600.
3 C. Yang and Z. Suo, *Nat. Rev. Mater.*, 2018, **3**, 125–142.
4 C. Zhang, B. Wu, Y. Zhou, F. Zhou, W. Liu and Z. Wang, *Chem. Soc. Rev.*, 2020, **49**, 3605–3637.
5 H. Yuk, B. Lu and X. Zhao, *Chem. Soc. Rev.*, 2019, **48**, 1642–1667.
6 Q. Ni, X. He, J. Zhou, Y. Yang, Z. Zeng, P. Mao, Y. Luo, J. Xu, B. Jiang, Q. Wu, B. Wang, Y. Qin, L. Gong, L. Tang and S. Li, *J. Mater. Sci. Technol.*, 2024, **191**, 181–191.
7 S. Li, Z. Yu, B. Guo, K. Guo, Y. Li, L. Gong, L. Zhao, J. Bae and L. Tang, *Nano Energy*, 2021, **90**, 106502.
8 S. Li, X. He, Z. Zeng, B. Jiang, Q. Wu, L. Gong, Y. Li, J. Bae, S. Wang and L. Tang, *Nano Energy*, 2022, **103**, 107789.
9 Y. Ye, Y. Zhang, Y. Chen, X. Han and F. Jiang, *Adv. Funct. Mater.*, 2020, **30**, 2003430.
10 B. Li, J. Liu, F. Lyu, Z. Deng, B. Yi, P. Du, X. Yao, G. Zhu, Z. Xu, J. Lu and Y. Y. Li, *Adv. Funct. Mater.*, 2021, **32**, 2109302.
11 B. Joos, J. Volders, R. R. da Cruz, E. Baeten, M. Safari, M. K. Van Bael and A. T. Hardy, *Chem. Mater.*, 2020, **32**, 3783–3793.
12 R. Li, T. Fan, G. Chen, K. Zhang, B. Su, J. Tian and M. He, *Chem. Mater.*, 2020, **32**, 874–881.
13 H. Qin, R. E. Owyeung, S. R. Sonkusale and M. J. Panzer, *J. Mater. Chem. C*, 2019, **7**, 601–608.
14 K. Fan, W. Wei, Z. Zhang, B. Liu, W. Feng, Y. Ma and X. Zhang, *Chem. Eng. J.*, 2022, **449**, 137878.
15 C. B. Kim, K. B. Jeong, B. J. Yang, J. W. Song, B. C. Ku, S. Lee, S. K. Lee and C. Park, *Angew. Chem., Int. Ed.*, 2017, **56**, 16180–16185.
16 R. Wang, S. Zhang, Y. Su, J. Liu, Y. Ying, F. Wang and X. Cao, *Electrochim. Acta*, 2017, **258**, 328–335.
17 K. Fan, L. Wang, W. Wei, F. Wen, Y. Xu, X. Zhang and X. Guan, *Chem. Eng. J.*, 2022, **441**, 136026.
18 C. Gu, Y. Peng, J. Li, H. Wang, X. Xie, X. Cao and C. Liu, *Angew. Chem., Int. Ed.*, 2020, **59**, 18768–18773.
19 Y. Liang, K. Wang, J. Li, H. Wang, X. Q. Xie, Y. Cui, Y. Zhang, M. Wang and C. Liu, *Adv. Funct. Mater.*, 2021, **31**, 2104963.
20 H. Sun, B. Zhang, L. Lu, Z. Chen, Y. Huo, W. Li, B. Zhang and J. Song, *Chem. Eng. J.*, 2023, **451**, 139051.
21 K. Wang, H. Wang, J. Li, Y. Liang, X. Q. Xie, J. Liu, C. Gu, Y. Zhang, G. Zhang and C. Liu, *Mater. Horiz.*, 2021, **8**, 2520–2532.
22 B. B. Hansen, S. Spittle, B. Chen, D. Poe, Y. Zhang, J. M. Klein, A. Horton, L. Adhikari, T. Zelovich, B. W. Doherty, B. Gurkan, E. J. Maginn, A. Ragauskas, M. Dadmun, T. A. Zawodzinski, G. A. Baker, M. E. Tuckerman, R. F. Savinell and J. R. Sangoro, *Chem. Rev.*, 2021, **121**, 1232–1285.
23 S. E. Hooshmand, R. Afshari, D. J. Ramón and R. S. Varma, *Green Chem.*, 2020, **22**, 3668–3692.
24 S. Wang, H. Cheng, B. Yao, H. He, L. Zhang, S. Yue, Z. Wang and J. Ouyang, *ACS Appl. Mater. Interfaces*, 2021, **13**, 20735–20745.
25 Z. Ma, J. Wang, Y. Deng, Y. Wang and L. Yan, *Biomacromolecules*, 2021, **22**, 4181–4190.
26 J. Wu, Q. Liang, X. Yu, Q. F. Lü, L. Ma, X. Qin, G. Chen and B. Li, *Adv. Funct. Mater.*, 2021, **31**, 2011102.
27 A. S. Hoffman, *Adv. Drug Delivery Rev.*, 2012, **64**, 18–23.
28 C. Keplinger, J.-Y. Sun, C. C. Foo, P. Rothemund, G. M. Whitesides and Z. Suo, *Science*, 2013, **341**, 984–987.
29 Y. Kitazawa, K. Ueno and M. Watanabe, *Chem. Rec.*, 2018, **18**, 391–409.
30 Y. Zhao, H. Cheng, Y. Li, J. Rao, S. Yue, Q. Le, Q. Qian, Z. Liu and J. Ouyang, *J. Mater. Chem. A*, 2022, **10**, 4222–4229.
31 C. Creton, *Macromolecules*, 2017, **50**, 8297–8316.
32 S. Wang and M. W. Urban, *Nat. Rev. Mater.*, 2020, **5**, 562–583.
33 R. Tamate, K. Hashimoto, T. Horii, M. Hirasawa, X. Li, M. Shibayama and M. Watanabe, *Adv. Mater.*, 2018, **30**, 1802792.
34 E. Kamio, T. Yasui, Y. Iida, J. P. Gong and H. Matsuyama, *Adv. Mater.*, 2017, **29**, 1704118.
35 H. Zhang, N. Tang, X. Yu, M. H. Li and J. Hu, *Adv. Funct. Mater.*, 2022, **32**, 2206305.
36 L. C. Tome and D. Mecerreyes, *J. Phys. Chem. B*, 2020, **124**, 8465–8478.
37 J. Wang, B. Zhan, S. Zhang, Y. Wang and L. Yan, *ACS Appl. Polym. Mater.*, 2022, **4**, 2057–2064.
38 T. Chen, X. Mai, L. Ma, Z. Li, J. Wang and S. Yang, *ACS Appl. Polym. Mater.*, 2022, **4**, 3982–3993.
39 T. Chen, R. Luo, Y. Liu, L. Ma, Z. Li, C. Tao, S. Yang and J. Wang, *ACS Appl. Mater. Interfaces*, 2022, **14**, 40276–40285.
40 S. Chen and J. Feng, *ACS Appl. Mater. Interfaces*, 2023, **15**, 44752–44762.
41 Y. Liang, D. Zou, Y. Zhang and Z. Zhong, *Chem. Eng. J.*, 2023, **475**, 145928.
42 C. Cai, H. Gong, S. Wu, F. Li, S. Liu, Z. Tan and S. Dong, *Chem. Eng. J.*, 2023, **451**, 138674.
43 Q. Lu, H. Li and Z. Tan, *ACS Appl. Mater. Interfaces*, 2023, **15**, 34055–34063.
44 R. Xue, N. Zhou, S. Yin, Z. Qian, Z. Dai and Y. Xiong, *Chem. Eng. J.*, 2023, **465**, 143072.
45 P. Wang, D. Pei, Z. Wang, M. Li, X. Ma, J. You and C. Li, *Chem. Eng. J.*, 2020, **398**, 125540.
46 P. Yao, Q. Bao, Y. Yao, M. Xiao, Z. Xu, J. Yang and W. Liu, *Adv. Mater.*, 2023, **35**, 2300114.
47 Q. Rong, W. Lei and M. Liu, *Chem.–Eur. J.*, 2018, **24**, 16930–16943.
48 Z. Liu, Y. Zheng, L. Jin, K. Chen, H. Zhai, Q. Huang, Z. Chen, Y. Yi, M. Umar, L. Xu, G. Li, Q. Song, P. Yue, Y. Li and Z. Zheng, *Adv. Funct. Mater.*, 2021, **31**, 2007622.
49 H. Liu, H. Zhang, W. Han, H. Lin, R. Li, J. Zhu and W. Huang, *Adv. Mater.*, 2021, **33**, 2004782.

